Conformation and dynamics of a self-avoiding active flexible polymer

Shalabh K. Anand[*] and Sunil P. Singh[†]

Department of Physics, Indian Institute of Science Education and Research, Bhopal 462 066, Madhya Pradesh, India

We investigate conformations and dynamics of a polymer considering its monomers to be active Brownian particles. This active polymer shows very intriguing physical behavior which is absent in an active Rouse chain. The chain initially shrinks with active force, which starts swelling on further increase in force. The shrinkage followed by swelling is attributed purely to excluded-volume interactions among the monomers. In the swelling regime, the chain shows a crossover from the self-avoiding behavior to the Rouse behavior with scaling exponent $\nu_a \approx 1/2$ for end-to-end distance. The nonmonotonicity in the structure is analyzed through various physical quantities; specifically, radial distribution function of monomers, scattering time, as well as various energy calculations. The chain relaxes faster than the Rouse chain in the intermediate force regime, with a crossover in variation of relaxation time at large active force as given by a power law $\tau_r \sim \text{Pe}^{-4/3}$ (Pe is Péclet number).

Introduction. A collection of freely moving active Brownian particles has drawn immense research activities in the past few years in view of interdisciplinary applications [1–6]. These individual agents ballistically propel themselves by conversion of chemical energy into mechanical energy, thus their motion can be controlled in experiments in a desired manner; consequently, they display rich collective dynamics [7–13]. A collection of such active particles connected via a linear chain exhibits numerous interesting features [14–23], which is often absent in passive systems. For example, an active chain exhibits shrinkage and swelling [24–31], spontaneous oscillations [32–34], enhanced diffusion [24–28], etc. The collective dynamics of such systems display various emergent structures; understanding them is a fundamental quest from a biophysics point of view as it poses a great challenge [35–43].

With the help of minimal models, the behavior of an active flexible chain or rigid filaments has been explored [24–28,34,44–64]. An accessible analytically tractable model for the polymer is the Rouse model, and inclusion of the activity in this model is studied in the literature [26–30,56,65]. An active Rouse chain shows swelling with a power-law scaling relation on active force with an exponent 1/3. Analytical calculations suggest that a flexible polymer always swells, whereas a semiflexible chain shrinks at smaller force, and in the asymptotic limit it swells analogous to an active Rouse chain with the same exponent [27,28,66]. The swelling of chain, relaxation, and its center-of-mass diffusion can be strongly influenced by the solvent properties and viscoelastic behavior of the medium [67,68]. The competition between elastic and self-avoiding forces causes shrinkage to a passive chain in an active bath in two spatial dimensions (2D) [58]. On the other hand a self-avoiding active chain in 2D shrinks, which is followed by swelling at larger active strength [59].

How excluded-volume interactions influence the structure of a chain in three dimensions (3D), its relaxation, and scaling exponents are important questions that have not been addressed very well in the previous studies.

The present work elucidates the role of excluded volume together with the activity on the relaxation and structure of the chain. In our simulations, we found that the end-to-end distance (R_e) and radius of gyration (R_g) of the chain shrinks in the intermediate range of active force (Pe) in the absence of hydrodynamics. In a recent study, it has been shown that the effect of hydrodynamics brings a similar behavior [30]. We analyze here the shrinkage of the chain through relaxation time, mean collision of monomers, radial distribution function, softness of the potential, and elastic and repulsive energies. The scaling exponent of the chain in stretching regime follows a power law on active force as $R_e \approx \text{Pe}^{1/3}$ and further with variation on the chain length as $R_e \approx N^{\nu_a}$, where $\nu_a \approx 1/2$ in the stretching regime.

Model. A flexible chain is composed of a linear sequence of N Brownian particles; the consecutive monomers in the chain are connected by harmonic potential $\Phi_h = \frac{k_s}{2} \sum_{i=1}^{N-1} (|\boldsymbol{r}_{i+1} - \boldsymbol{r}_i| - l_0)^2$, where $\boldsymbol{r}_i$, l_0, and k_s denote the position of the ith monomer, the average equilibrium bond length, and the spring constant, respectively. The excluded-volume potential restricts overlapping of beads in a polymer, and it is implemented here as the standard repulsive part of Lennard-Jones interactions for shorter distance, i.e., $R_{ij} < 2^{1/6}\sigma$,

$$u_{ij} = 4\epsilon \left[\left(\frac{\sigma}{R_{ij}} \right)^{12} - \left(\frac{\sigma}{R_{ij}} \right)^{6} \right] + \epsilon, \qquad (1)$$

and for $R_{ij} \geqslant 2^{1/6}\sigma$, $u_{ij} = 0$, where $\boldsymbol{R}_{ij} = \boldsymbol{r}_j - \boldsymbol{r}_i$, ϵ is interaction energy, and σ is the diameter of the monomer. The total Lennard-Jones (LJ) energy can be expressed as $\Phi_{\text{LJ}} = \sum_{i=1}^{N-1} \sum_{j=i+1}^{'N} u_{ij}$. The prime in the second summation excludes the LJ interaction between consecutive bonded neighbors.

[*]skanand@iiserb.ac.in
[†]spsingh@iiserb.ac.in
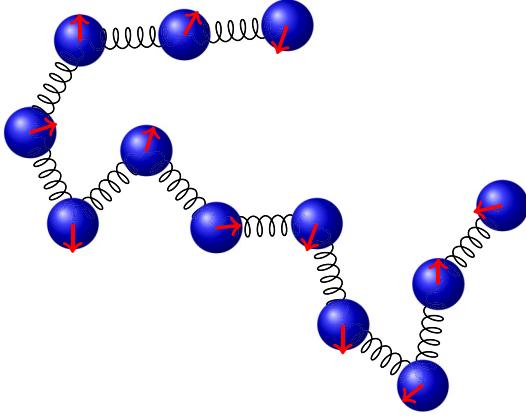
FIG. 1. A pictorial snapshot of a modeled polymer. Arrow indicates the direction of active force on the corresponding monomer.

The equation of motion of an active Brownian bead of the polymer chain in an overdamped limit is

$$\gamma \frac{d\mathbf{r}_i}{dt} = -\nabla_i \Phi + \mathbf{F}_r^i + F_a \hat{\mathbf{u}}_i, \quad (2)$$

where γ is the friction coefficient, $\mathbf{F}_r^i$ is the thermal noise with zero mean, and F_a is the strength of self-propulsion force exerted on the ith bead along the $\hat{\mathbf{u}}_i$ direction. The viscous drag and the thermal noise obey the fluctuation-dissipation relation $\langle \mathbf{F}_r^i(t) \cdot \mathbf{F}_r^j(t') \rangle = 6 k_B T \gamma \delta_{ij} \delta(t - t')$. The long-range hydrodynamic interactions are neglected here.

Active Brownian beads are modeled as polar molecules; their orientations $\hat{\mathbf{u}}_i$ are described by the rotational counterpart of the Langevin equation,

$$\gamma_r \frac{d\hat{\mathbf{u}}_i}{dt} = \boldsymbol{\zeta}_i \times \hat{\mathbf{u}}_i. \quad (3)$$

Here $\boldsymbol{\zeta}_i$ is a random torque with zero mean and variance $\langle \boldsymbol{\zeta}(t) \otimes \boldsymbol{\zeta}(t') \rangle = 2(k_B T)^2 \delta(t - t')/D_r$, and γ_r is the rotational friction coefficient given as $\gamma_r = k_B T/D_r$. The rotational diffusion is expressed in terms of translational diffusion (D_m) as $D_r = 3D_m/l_0^2$. The strength of active force is presented here as a ratio of active force with thermal force given as Pe $= (F_a l_0)/(k_B T)$, with Péclet number Pe as a dimensionless quantity. A schematics of the polymer chain is displayed in Fig. 1, where arrows show the direction of active force on monomers.

All the physical parameters presented in this Rapid Communication are scaled in units of the bond length l_0, diffusion coefficient of a monomer D_m, and thermal energy $k_B T$. Simulations are performed in cubic periodic boxes in three spatial dimensions; polymer length is varied in the range of $N = 50$–300. Other parameters are chosen as k_s in the range of 10^3–10^4 in units of $k_B T/l_0^2$, $\epsilon/k_B T = 1$, and time is in units of $\tau = l_0^2/D_m$. For higher Pe, larger values of k_s are chosen to avoid stretching of bonds. The monomer size σ is varied in the range of $\sigma/l_0 = 0.2$–1.0 and Pe is varied in the range of 0–1000. We use the Euler integration technique to solve Eqs. (2) and (3) with time step Δt in the range of $10^{-3}\tau$–$10^{-5}\tau$ to ensure stable simulation results. In order to obtain better statistics, each data point is averaged over 20 independent simulations.

Structural properties. There is vast literature on the equilibrium behavior of a polymer chain [69–77] followed by extension to an active chain [24,60,78]. We present the effect of active noise on the structure of a self-avoiding chain in the form of radius-of-gyration, end-to-end distance and its distribution, pair-correlation function, and scaling behaviors.

The quantification of structural change is analyzed in terms of end-to-end distance R_e and radius of gyration R_g as

$$R_e^2 = \langle (\mathbf{r}_1 - \mathbf{r}_N)^2 \rangle; \quad R_g^2 = \frac{1}{N} \left\langle \sum_{i=1}^{N} (\mathbf{r}_i - \mathbf{R}_{cm})^2 \right\rangle, \quad (4)$$

where $\mathbf{R}_{cm}$ is the center of mass of the chain and the angular brackets indicate ensemble average. The computed R_e is displayed in Fig. 2(a), which reflects a significant shrinkage of polymer with Pe in the range of Pe < 50 for $N > 50$. The initial shrinkage of the chain is followed by stretching in the range of Pe > 50 as Fig. 2(a) illustrates. The swelling behavior of R_e appears quite alike to the Rouse chain. The normalized end-to-end distance for various chain lengths follows the same trend with relatively higher compression for large chain lengths. In the stretching regime, R_e follows a power-law variation on the Péclet number given by $R_e^2 \sim \text{Pe}^{2/3}$ with an exponent 2/3 identical to the Rouse chain [27,55,58].

Now, we turn our attention to scaling exponents ν_a of the chain in various regimes. The inset of Fig. 2(a) compares various plots of R_e as a function of chain length at Pe $= 0$, 15, 70, 150, and 200. These curves indicate a variation of the scaling exponents ν_a with Pe. It clearly suggests that for $1 < \text{Pe} < 50$, the exponent is slightly smaller than 3/5; for comparison, a solid line is drawn in the inset of Fig. 2(a) at $\nu_a = 3/5$. A dashed line illustrates the variation of $R_e \sim N^{\nu_a}$ with $\nu_a = 1/2 \pm 0.05$. For Pe > 100, the exponent ν_a of the chain approaches the Rouse regime $\nu_a = 1/2$. To summarize the results in compression regime (triangle and diamond), we found that ν_a is smaller than 3/5 and slightly larger than 1/2.

The shrinkage of the active chain is visible in the probability distribution of R_e. Figure 2(b) reflects a shift in the location of the peak with propulsion strength Pe at a fixed chain length $N = 200$. The peak shifts weakly towards left for the smaller values of Pe with a shape almost identical to the passive polymer. The initial shift of the peak towards small R_e changes its course of variation with shifting towards the right for large Pe. The change in distribution is consistent with the nonmonotonicity in the structure. The end-to-end distance and probability distribution confirms the compression in the intermediate regime, i.e., $1 < \text{Pe} < 50$.

In order to bridge the gap between monotonic swelling of an active Rouse chain and the nonmonotonic behavior of an excluded-volume chain, we quantify R_e of the chain by varying monomer's diameter σ. Figure 2(c) illustrates the normalized end-to-end distance $R_e^2/R_{e,0}^2$ with respect to its passive counterpart $R_{e,0}^2$ as a function of Pe. Our simulations reveal that in the diameter range 0.2–1.0, we are able to find a smooth transition from ideal to self-avoiding regime. For $\sigma = 0.2$, R_e displays a monotonic swelling with Pe, and the relative variations of R_e are identical to the Rouse behavior. A further increase in σ displays the shrinkage in the chain. In the intermediate regime of Pe, the relative compression of the chain grows with σ [see Fig. 2(c)]. The plot reveals a
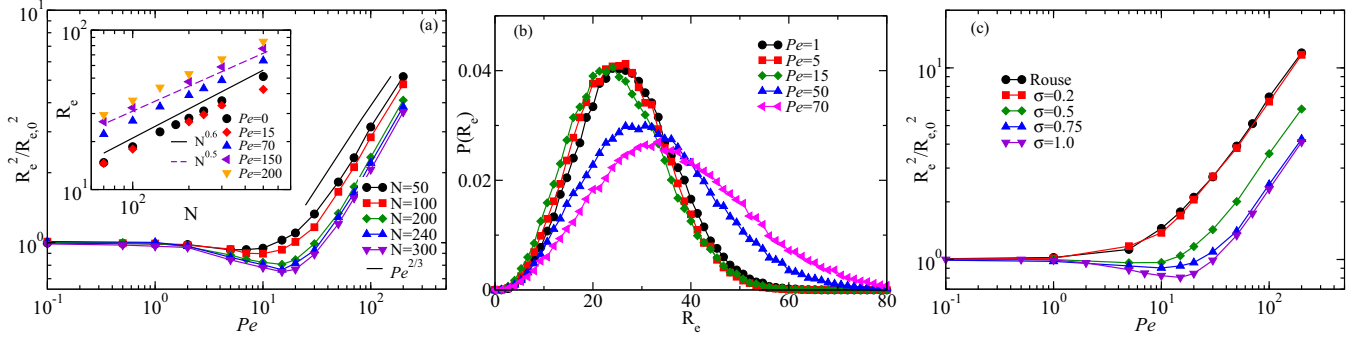
FIG. 2. (a) Relative variation of mean-square end-to-end distance ($R_e^2/R_{e,0}^2$) of the chain as a function of Pe for various chain lengths. Solid line shows a power-law variation $Pe^{2/3}$. The inset shows R_e with N at Pe = 0, 15, 70, 150, and 200, at $\sigma = 1$. The solid and dashed lines are showing power-law variation at exponents $\nu_a = 3/5$ and $1/2$, respectively. (b) The distribution of end-to-end distance at $N = 200$ and $\sigma = 1$. (c) Relative variation of end-to-end distance ($R_e^2/R_{e,0}^2$) of an active chain with $N = 200$ as a function of Pe for various monomer diameters $\sigma = 0.2, 0.5, 0.75,$ and 1.0, and the Rouse chain (bullet).

change in behavior from the continuous swelling regime to a shrinkage followed by swelling with variation in σ. This effect is attributed to the increase in multibody interactions with monomer diameter. This effect is discussed later in this Rapid Communication and shows how active noise influences the scattering time.

The compression of the chain indicates a rise in local crowding in the intermediate regime $1 < \text{Pe} < 50$. To unveil this behavior, we estimate radial distribution function, which is a measure of average local density around a monomer. It is defined here as $g(r) = n(r)/(4\pi r^2 dr\rho_0)$; here $n(r)$ is the average number of monomers with respect to a given monomer in a concentric shell of radius r and thickness dr. We have considered the monomer density to be $\rho_0 = 7 \times 10^{-6}$, which is very small in dilute concentrations of polymer, thus we present a scaled radial distribution $g'(r) = \rho_0 g(r)$ in the plot for better visualization. Figure 3 displays the radial distribution function of a chain; it clearly reveals a pronounced variation in the height of peaks relative to the passive chain. Hence, it shows higher local density in the intermediate Pe regime, causing shrinkage of the chain. The height of peaks in distribution reverts its behavior for higher Pe strengths and eventually becomes smaller than the passive chain. In this
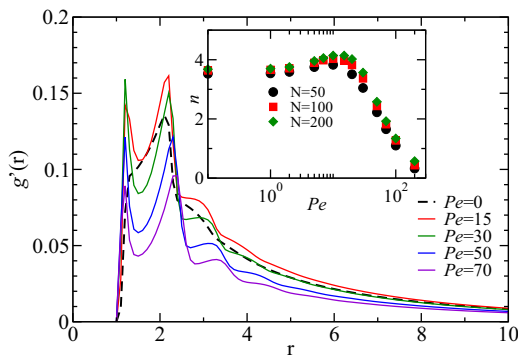
limit, the number of neighbors is less relative to the passive chain as evident from its extension.

The variation in local coordination number in the intermediate range of the Péclet number can be estimated from the radial distribution function as $n = \int_0^{R_{\text{cut}}} 4\pi r^2 g(r) dr$, where R_{cut} is taken up to the second peak at Pe = 0, which is $R_{\text{cut}} = 2.25$. This gives the average coordination number of the chain in a cut-off distance (R_{cut}) as a function of Pe (see inset of Fig. 3). The local coordination number grows with Pe in the cut-off distance, which indicates local accumulation of monomers and thus suggests shrinkage of the chain. In the limit of Pe $\gg$ 1, the local density declines, thereby it signifies the stretching of chain.

Dynamics. The understanding of nonmonotonic behavior of an active polymer's structure becomes more evident when we quantify average collision time t_c, and compare it with various monomer sizes. The overlap of two monomer's positions in the range of $R_c \leqslant 2^{1/6}\sigma$ (LJ cut-off) is defined to be a collision event. The average collision time provides a measure of hindrance or obstruction in motion of a monomer in the presence of self-avoidance. Figure 4(a) shows a decrease in collision time t_c followed by an increase with Pe for $\sigma = 0.5, 0.75,$ and 1.0. This is due to an increase in local density and speed of monomers with increasing activity in the range $0 < \text{Pe} < 50$. Further, they start dispersing far from each other on higher strength of Pe as already pointed in radial distribution. With higher strength (Pe), collision becomes frequent as expected from the kinetic theory $t_c \sim \frac{1}{v_r}$; v_r reads as the average relative speed of monomers. The onset of an increase of t_c appears nearly at the same Pe as the onset of R_e and R_g (see Fig. SI-1(a) in the Supplemental Material [79]). With an increase in active fluctuations, the polymer gets stretched, thus the frequency of collision goes down, hence t_c (collision time) goes up as Fig. 4(a) reflects. The effect of monomer size on scattering time indicates variation in an active polymer's conformation from self-avoiding to ideal behavior. A smaller monomer has a larger collision time as it exhibits a smaller scattering cross section ($b = \pi\sigma^2$), which is reflected in Fig. 4(a). It is noteworthy that the relative variation in t_c/t_0 for small $\sigma = 0.5$ has strikingly significant variation, importantly in the intermediate regime of Pe as the inset in

FIG. 3. Radial distribution of the chain for various Pe at $N = 200$, $\sigma = 1$, and number density $\rho_0 = 7 \times 10^{-6}$, with $g'(r) = \rho_0 g(r)$. Inset displays average coordination number n in the first two shells ($R_{\text{cut}} = 2.25$) as a function of Pe for $N = 50, 100,$ and 200.
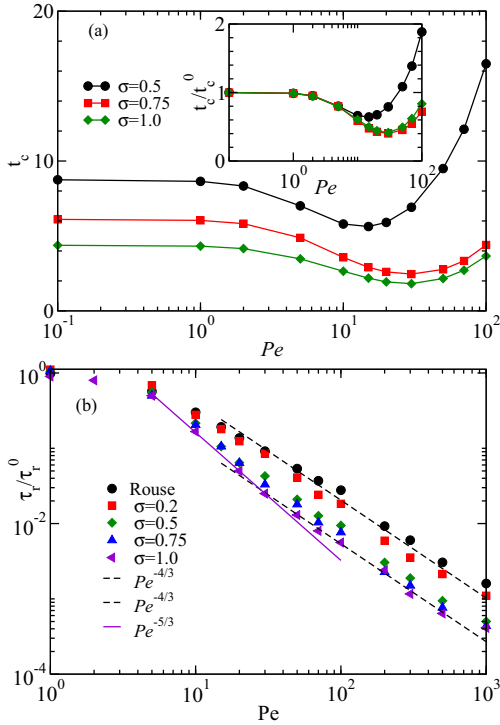
FIG. 4. (a) Average collision time t_c of monomers as a function of Pe for $N = 200$. Inset shows the relative variation of t_c/t_c^0 with Pe; here t_c^0 is for Pe = 0. (b) The relative variation of relaxation time τ_r/τ_r^0 for various monomer diameters σ as a function of Pe at $N = 200$. The dashed and solid lines show the power-law variation with exponents 4/3 and 5/3, respectively.

Fig. 4(a) reflects. The depth in t_c/t_0 ($10 < $ Pe $ < 50$) becomes shallow with σ, which diminishes in the asymptotic limit of $\sigma \to 0$.

To enlighten the difference in relaxation behavior of a Rouse and a self-avoiding active chain, we compute the end-to-end correlation of the polymer. The end-to-end correlation follows an exponential decay (in longer time $\gamma_r t \gg 1$), $\langle \boldsymbol{R}_e(0) \cdot \boldsymbol{R}_e(t) \rangle \simeq \exp(-t/\tau_r)$, with τ_r as the longest relaxation time of a polymer. The estimated relaxation time τ_r/τ_r^0 from the correlation is displayed in Fig. 4(b). It presents a relative variation of τ_r with respect to that of the passive chain τ_r^0 for various monomer diameters, along with the Rouse chain. In the limit of smaller monomer size, we achieve relaxation behavior of the Rouse chain with pronounced variation in τ_r. The relaxation behavior indicates a power-law variation given as $\tau_r \approx \mathrm{Pe}^{-\beta_a}$, for the Rouse chain $\beta_a \approx 4/3$. The self-avoiding chain exhibits a very intriguing feature with a sharp variation of τ_r in the limit Pe < 100. The scaling exponent is found to be $\beta_a \approx 5/3$ [see the solid line in Fig. 4(b)]. A crossover from the sharp relative variation ($\beta_a \approx 5/3$ for Pe < 100) to the exponent $\beta_a = 4/3$ is observed in the limit of Pe > 100. More importantly the variation in relaxation with Pe becomes faster in the compression regime. The larger relative change in the relaxation time in the presence of hydrodynamics than in the Rouse chain is also reported in Ref. [66], where it was shown that the competition between active force and the variation in τ_r controls the structure leading to compression of the chain. The relatively faster variation
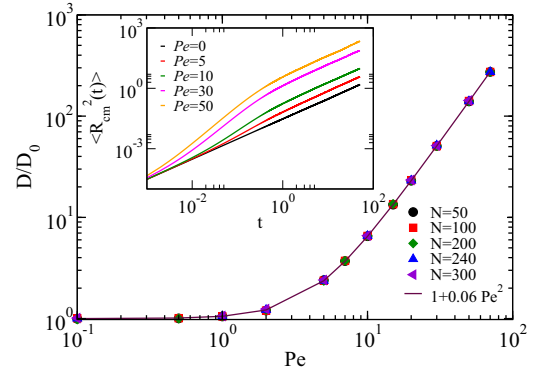
FIG. 5. The effective diffusion coefficient as a function of Pe for various chain lengths. Inset shows mean-squared displacement of the chain for $N = 200$ for various Pe at $\sigma = 1$.

of τ_r obtained in our simulations for the self-avoiding chain resembles the results of Ref. [66]. A smooth variation in τ_r from the self-avoiding chain to the Rouse chain is obtained by a variation in monomer size as Fig. 4(b) illustrates in various plots.

In this section, diffusion of the active chain is presented through mean-squared displacement (MSD) of the center-of-mass (COM) of the chain. The long-time MSD of the COM is expressed as $\langle R_{\mathrm{cm}}(t)^2 \rangle = \langle [r_{\mathrm{cm}}(t) - r_{\mathrm{cm}}(0)]^2 \rangle$. The MSD shows the ballistic motion $\langle R_{\mathrm{cm}}^2(t) \rangle \sim t^2$ in the short-time and diffusive regime $\langle R_{\mathrm{cm}}^2(t) \rangle = 6Dt$ in the long-time limit. The inset of Fig. 5 displays the MSD of the chain at various Pe = 0, 5, 10, 30, and 50, and it clearly indicates enhanced diffusion with Pe. This can be understood in terms of the drag of monomers through active forces in random directions, which causes faster movement relative to the passive monomers resulting in enhanced MSD of the chain with Pe. The self-diffusion coefficient D/D_0 obtained from diffusive regime is displayed in Fig. 5. The effective diffusivity increases quadratically as $D \sim \mathrm{Pe}^2$. Moreover as expected, D is independent of the chain length when scaled by the diffusion coefficient of the passive chain (D_0, at Pe = 0), thus we can express $D = D_0(1 + a\mathrm{Pe}^2)$, where $a \approx 0.06$ is a constant. The effective diffusion can be used to define the effective temperature of the chain as $T_{\mathrm{eff}} = 1 + a\mathrm{Pe}^2$. In particular cases, this expression is argued to be identical to a passive system with temperature equivalent to T_{eff} [80–82]. However, mapping of the effective temperature of the active polymer to temperature would not be sufficient for all physical behaviors.

The segmental MSD of the chain reveals internal dynamics, specifically the subdiffusive behavior in the intermediate time limit (10^{-1}–10^2). The crossover from subdiffusive to diffusive survives relatively at longer time for larger chain in a broad window of Pe [see Supplemental Material Figs. SI-2(a) and SI-2(b)]. This enlightens the internal dynamical picture of a chain in the discussed parameter space.

Discussion and summary. In summary, we have unveiled the effect of excluded-volume interactions on the structural properties and internal dynamics of an active polymer in 3D. A polymer shrinks in the presence of activity, which is

followed by swelling. A pronounced nonmonotonic behavior in R_e is depicted in a broad range of activity strength for larger chain lengths. This compression is more pronounced in 2D [57]. We have shown that in the limit of Pe < 50, the compression is primarily a consequence of the interaction of monomers with its neighbors, which brings an increase in local density.

This increase can be understood in terms of rotational diffusion which requires $1/D_r$ time to change the monomer orientations to escape from the local environment. The radial distribution function substantiates the effect of softness and the increase in local density. The softness of repulsive potential exhibits a weak contribution in the structure at large active forces. A systematic study on the softness of the potential due to activity is taken into account here by varying ϵ over a range of 10–10^{-3}. A larger epsilon corresponds to a stiffer potential, which exhibits a very nominal change in the values with preserving the qualitative behavior. On the other hand, relatively softer potentials lead to a significant change in R_e^2 with activity (see Fig. SI-3). We have also tested our results for a different potential which looks similar in nature to the LJ potential but steeper. This potential also exhibits a nonmonotonic behavior in structure.

The fast random motion of monomers results in stretching of the chain for large Pe > 50, thereby an increase in the elastic energy. Interestingly, the power-law scaling exponent of the self-avoiding chain ($R_e \approx N^{\nu_a}$) ν_a becomes smaller in this regime and approaches the Rouse limit ($\nu_a = 1/2$), despite stretching of the polymer due to activity. In addition, the longest relaxation decreases with power law as $\tau_r \approx$ Pe$^{-\beta_a}$, for the Rouse and self-avoiding chains in the large Pe limit with exponent $\beta_a \approx 4/3$. The relaxation behavior of the self-avoiding chain exhibits a crossover from the exponent $\beta_a \approx 5/3$ to $4/3$ with Pe. In conclusion, the role of self-avoidance has been explored in a systematic way by varying the monomer's diameter that bridges the gap between an excluded volume chain and a Rouse chain; consequently it connects the variation of numerous physical properties such as R_e, τ_r, and scattering time smoothly from one to another limit. The effect of excluded volume is substantial in the flexible limit, which slowly diminishes with semiflexibility of the chain [83]. A theoretical approach for the radius of gyration and relaxation time of the excluded volume chain would be essential for a complete understanding of the system. In addition, a detailed study on the softness of potential and the effect of rotational diffusion on the structure of an active chain would be interesting to investigate further.

[1] T. Vicsek, A. Czirók, E. Ben-Jacob, I. Cohen, and O. Shochet, Phys. Rev. Lett. **75**, 1226 (1995).

[2] M. C. Marchetti, J.-F. Joanny, S. Ramaswamy, T. B. Liverpool, J. Prost, M. Rao, and R. A. Simha, Rev. Mod. Phys. **85**, 1143 (2013).

[3] J. Elgeti, R. G. Winkler, and G. Gompper, Rep. Prog. Phys. **78**, 056601 (2015).

[4] C. Bechinger, R. Di Leonardo, H. Löwen, C. Reichhardt, G. Volpe, and G. Volpe, Rev. Mod. Phys. **88**, 045006 (2016).

[5] J. Toner and Y. Tu, Phys. Rev. Lett. **75**, 4326 (1995).

[6] C. Dombrowski, L. Cisneros, S. Chatkaew, R. E. Goldstein, and J. O. Kessler, Phys. Rev. Lett. **93**, 098103 (2004).

[7] J. Palacci, S. Sacanna, A. P. Steinberg, D. J. Pine, and P. M. Chaikin, Science **339**, 936 (2013).

[8] D. P. Singh, U. Choudhury, P. Fischer, and A. G. Mark, Adv. Mater. **29**, 1701328 (2017).

[9] J. Arlt, V. A. Martinez, A. Dawson, T. Pilizota, and W. C. Poon, Nat. Commun. **9**, 768 (2018).

[10] F. A. Lavergne, H. Wendehenne, T. Bäuerle, and C. Bechinger, Science **364**, 70 (2019).

[11] C. Lozano, B. Ten Hagen, H. Löwen, and C. Bechinger, Nat. Commun. **7**, 12828 (2016).

[12] B. Liebchen and H. Loöwen, Acc. Chem. Res. **51**, 2982 (2018).

[13] N. Yu, X. Lou, K. Chen, and M. Yang, Soft Matter **15**, 408 (2019).

[14] B. Biswas, R. K. Manna, A. Laskar, P. S. Kumar, R. Adhikari, and G. Kumaraswamy, ACS Nano **11**, 10025 (2017).

[15] D. Nishiguchi, J. Iwasawa, H.-R. Jiang, and M. Sano, New J. Phys. **20**, 015002 (2018).

[16] R. Di Leonardo, Nat. Mater. **15**, 1057 (2016).

[17] J. Yan, M. Han, J. Zhang, C. Xu, E. Luijten, and S. Granick, Nat. Mater. **15**, 1095 (2016).

[18] D. J. Ashton, R. L. Jack, and N. B. Wilding, Soft Matter **9**, 9661 (2013).

[19] D. Nykypanchuk, M. M. Maye, D. Van Der Lelie, and O. Gang, Nature (London) **451**, 549 (2008).

[20] Q. Chen, S. C. Bae, and S. Granick, Nature (London) **469**, 381 (2011).

[21] Y. Sasaki, Y. Takikawa, V. S. Jampani, H. Hoshikawa, T. Seto, C. Bahr, S. Herminghaus, Y. Hidaka, and H. Orihara, Soft Matter **10**, 8813 (2014).

[22] L. M. Ramírez, C. A. Michaelis, J. E. Rosado, E. K. Pabón, R. H. Colby, and D. Velegol, Langmuir **29**, 10340 (2013).

[23] H. Löwen, Europhys. Lett. **121**, 58001 (2018).

[24] S. K. Anand and S. P. Singh, Phys. Rev. E **98**, 042501 (2018).

[25] V. Bianco, E. Locatelli, and P. Malgaretti, Phys. Rev. Lett. **121**, 217802 (2018).

[26] N. Samanta and R. Chakrabarti, J. Phys. A: Math. Theor. **49**, 195601 (2016).

[27] T. Eisenstecken, G. Gompper, and R. G. Winkler, Polymers **8**, 304 (2016).

[28] T. Eisenstecken, G. Gompper, and R. G. Winkler, J. Chem. Phys. **146**, 154903 (2017).

[29] D. Osmanović and Y. Rabin, Soft Matter **13**, 963 (2017).

[30] A. Martín-Gómez, G. Gompper, and R. Winkler, Polymers **10**, 837 (2018).

[31] J. Shin, A. G. Cherstvy, W. K. Kim, and R. Metzler, New J. Phys. **17**, 113008 (2015).

[32] R. Chelakkot, A. Gopinath, L. Mahadevan, and M. F. Hagan, J. R. Soc., Interface **11**, 20130884 (2014).

[33] A. Laskar, R. Singh, S. Ghose, G. Jayaraman, P. S. Kumar, and R. Adhikari, Sci. Rep. **3**, 1964 (2013).

[34] S. K. Anand, R. Chelakkot, and S. P. Singh, Soft Matter **15**, 7926 (2019).

[35] O. C. Rodriguez, A. W. Schaefer, C. A. Mandato, P. Forscher, W. M. Bement, and C. M. Waterman-Storer, Nat. Cell Biol. **5**, 599 (2003).

[36] T. Vicsek and A. Zafeiris, Phys. Rep. **517**, 71 (2012).

[37] M. Abkenar, K. Marx, T. Auth, and G. Gompper, Phys. Rev. E **88**, 062314 (2013).

[38] S. J. DeCamp, G. S. Redner, A. Baskaran, M. F. Hagan, and Z. Dogic, Nat. Mater. **14**, 1110 (2015).

[39] Y. Sumino, K. H. Nagai, Y. Shitaka, D. Tanaka, K. Yoshikawa, H. Chaté, and K. Oiwa, Nature (London) **483**, 448 (2012).

[40] V. Schaller and A. R. Bausch, Proc. Natl. Acad. Sci. **110**, 4488 (2013).

[41] A. Ravichandran, Ö. Duman, M. Hoore, G. Saggiorato, G. A. Vliegenthart, T. Auth, and G. Gompper, eLife **8**, e39694 (2019).

[42] Ö. Duman, R. E. Isele-Holder, J. Elgeti, and G. Gompper, Soft Matter **14**, 4483 (2018).

[43] K. R. Prathyusha, S. Henkes, and R. Sknepnek, Phys. Rev. E **97**, 022606 (2018).

[44] R. G. Winkler, J. Elgeti, and G. Gompper, J. Phys. Soc. Jpn. **86**, 101014 (2017).

[45] V. Schaller, C. Weber, C. Semmrich, E. Frey, and A. R. Bausch, Nature (London) **467**, 73 (2010).

[46] J. Prost, F. Jülicher, and J.-F. Joanny, Nat. Phys. **11**, 111 (2015).

[47] A. Doostmohammadi, T. N. Shendruk, K. Thijssen, and J. M. Yeomans, Nat. Commun. **8**, 15326 (2017).

[48] F. Ndlec, T. Surrey, A. C. Maggs, and S. Leibler, Nature (London) **389**, 305 (1997).

[49] S. K. Anand and S. P. Singh, Soft Matter **15**, 4008 (2019).

[50] R. K. Manna and P. S. Kumar, Soft Matter **15**, 477 (2019).

[51] S. Ganguly, L. S. Williams, I. M. Palacios, and R. E. Goldstein, Proc. Natl. Acad. Sci. USA **109**, 15109 (2012).

[52] Y. Harada, A. Noguchi, A. Kishino, and T. Yanagida, Nature (London) **326**, 805 (1987).

[53] F. Juelicher, K. Kruse, J. Prost, and J.-F. Joanny, Phys. Rep. **449**, 3 (2007).

[54] M. Foglino, E. Locatelli, C. Brackley, D. Michieletto, C. Likos, and D. Marenduzzo, Soft Matter **15**, 5995 (2019).

[55] A. Ghosh and N. Gov, Biophys. J. **107**, 1065 (2014).

[56] M. S. E. Peterson, M. F. Hagan, and A. Baskaran, J. Stat. Mech.: Theory Exp. (2020) 013216.

[57] A. Kaiser and H. Löwen, J. Chem. Phys. **141**, 044903 (2014).

[58] J. Harder, C. Valeriani, and A. Cacciuto, Phys. Rev. E **90**, 062312 (2014).

[59] A. Kaiser, S. Babel, B. ten Hagen, C. von Ferber, and H. Löwen, J. Chem. Phys. **142**, 124905 (2015).

[60] R. E. Isele-Holder, J. Elgeti, and G. Gompper, Soft Matter **11**, 7181 (2015).

[61] R. E. Isele-Holder, J. Jäger, G. Saggiorato, J. Elgeti, and G. Gompper, Soft Matter **12**, 8495 (2016).

[62] A. Laskar and R. Adhikari, New J. Phys. **19**, 033021 (2017).

[63] H. Jiang and Z. Hou, Soft Matter **10**, 1012 (2014).

[64] S. Das and A. Cacciuto, Phys. Rev. Lett. **123**, 087802 (2019).

[65] D. Osmanović, J. Chem. Phys. **149**, 164911 (2018).

[66] A. Martín-Gómez, T. Eisenstecken, G. Gompper, and R. G. Winkler, Soft Matter **15**, 3957 (2019).

[67] H. Vandebroek and C. Vanderzande, Phys. Rev. E **92**, 060601(R) (2015).

[68] H. Vandebroek and C. Vanderzande, J. Stat. Phys. **167**, 14 (2017).

[69] R. G. Winkler, P. Reineker, and L. Harnau, J. Chem. Phys. **101**, 8119 (1994).

[70] L. Harnau, R. G. Winkler, and P. Reineker, J. Chem. Phys. **106**, 2469 (1997).

[71] O. Kratky and G. Porod, J. Colloid Sci. **4**, 35 (1949).

[72] N. Saitô, K. Takahashi, and Y. Yunoki, J. Phys. Soc. Jpn. **22**, 219 (1967).

[73] H.-P. Hsu, W. Paul, and K. Binder, Europhys. Lett. **92**, 28003 (2010).

[74] H.-P. Hsu, W. Paul, and K. Binder, Europhys. Lett. **95**, 68004 (2011).

[75] M. Doi and S. F. Edwards, *The Theory of Polymer Dynamics* (Oxford University Press, New York, 1988), Vol. 73.

[76] M. Rubinstein and R. H. Colby, *Polymer Physics* (Oxford University Press, 2003).

[77] M. Muthukumar, *Polymer Translocation* (CRC Press, Boca Raton, FL, 2016).

[78] Y. Man and E. Kanso, Soft Matter **15**, 5163 (2019).

[79] See Supplemental Material at http://link.aps.org/supplemental/10.1103/PhysRevE.101.030501 for MSD of the monomer and structural properties for various potentials.

[80] J. Palacci, C. Cottin-Bizonne, C. Ybert, and L. Bocquet, Phys. Rev. Lett. **105**, 088304 (2010).

[81] D. Loi, S. Mossa, and L. F. Cugliandolo, Soft Matter **7**, 3726 (2011).

[82] D. Loi, S. Mossa, and L. F. Cugliandolo, Soft Matter **7**, 10193 (2011).

[83] T. Eisenstecken, A. Ghavami, A. Mair, G. Gompper, and R. G. Winkler, in *Conformational and Dynamical Properties of Semiflexible Polymers in the Presence of Active Noise AIP Conf. Proc. No. 1871* (AIP, New York, 2017), p. 050001.